



Cite this: *Chem. Sci.*, 2020, **11**, 3124

All publication charges for this article have been paid for by the Royal Society of Chemistry

Received 24th December 2019

Accepted 1st March 2020

DOI: 10.1039/c9sc06505a

rsc.li/chemical-science

## 1. Introduction

Heterogeneous catalysis is widely used in solar-driven water splitting,  $\text{CO}_2/\text{N}_2$  reduction, fuel cells, pollutant degradation, fine chemical production and biomass detection, which are closely related to public issues of worldwide concern such as energy conversion, environmental remediation, health monitoring and chemical synthesis.<sup>1–4</sup> Compared with homogeneous catalysis, heterogeneous catalysis possesses prominent

College of Chemistry, Chemical Engineering and Materials Science, Soochow University, Suzhou 215123, P. R. China. E-mail: xjfeng@suda.edu.cn



Liping Chen is a researcher at Soochow University. He obtained his B.S. degree (2009) from Jilin University, China and received his PhD (2014) from the College of Chemistry, Jilin University. He worked as a Postdoctoral Research Fellow at Soochow University (2015–2018) under the direction of Prof. Xinjian Feng. His current research focuses on design and fabrication of biomimetic interfacial electrodes for photoelectrochemical and biosensor applications.

advantages in reactant diversification and catalytic separation/regeneration. However, the kinetics and selectivity of catalytic reactions that take place at a liquid–solid diphase interface can be restricted by the low solubility and slow diffusion rate of gaseous reactants in the liquid phase when gaseous reactants are involved in aqueous heterogeneous reactions (such as catalytic  $\text{O}_2$  reduction reaction,  $\text{CO}_2$  reduction reaction, and  $\text{N}_2$  fixation). Although gas pre-saturation and/or continuous ventilation can address this issue, the essential problem remains unsolved: the low catalytic kinetics originating from the slow gas transport to the reaction centre cannot be increased. As



Xinjian Feng is a Professor in the Department of Chemistry at Soochow University. Prior to his appointment, he was a professor at the Suzhou Institute of Nanotech and Nanobionics, CAS. Before moving to Suzhou, he worked as a Humboldt Fellow at the Erlangen University of Germany and a postdoc at the Penn State University in America. He received his doctoral degree from the Institute of Chemistry, CAS. His current scientific interests mainly focus on the construction and application of triphase reaction interfaces for environmental remediation, health monitoring and energy conversion.



a result, the performance of various systems based on conventional diphase catalytic reactions is generally limited.

Inspired by natural surfaces with non-wetting features, artificial superhydrophobic substrates have been constructed based on the cooperative effect between micro-/nanocomposite surface structures and low surface energy materials.<sup>5</sup> When these substrates are immersed in an aqueous solution, gas pockets will be trapped inside the rough surface structures leading to the formation of an air–liquid–solid triphase joint interface.<sup>6</sup> In this triphase interface, gaseous reactants can be readily delivered to the catalytic centre from the air phase with continuous and sufficient supply—this eliminates the gas transport problem in traditional diphase systems and can boost the catalytic kinetics in heterogeneous reactions.

In this minireview, we focus on recent studies on the design and construction of air–liquid–solid triphase reaction interfaces and their effect on gas consumption related photocatalytic reactions, (photo)electrochemical reactions, and enzymatic reactions. By analysing the promoting effect of the triphase architecture in these reactions, we strive to help our readers construct a new concept of triphase reaction systems for improving the reaction efficiency and selectivity in gaseous reactant-based reactions with applications in environmental remediation, clean energy production, and health monitoring.

## 2. O<sub>2</sub> consumption reactions with triphase interfaces

### 2.1 Photocatalytic reactions

Semiconductor-based photocatalysis with electron reduction or hole oxidation has attracted considerable interest. However, the separation of photogenerated electrons and holes is an essential factor that affects the reaction efficiency. When gaseous reactants are involved in photocatalytic reactions such as H<sub>2</sub>O<sub>2</sub> production and organic pollutant degradation by O<sub>2</sub> reduction, the solubility and diffusion rate of O<sub>2</sub> are key issues that restrict the reaction rate and substrate–product conversion efficiency. Here, we describe the application of the air–liquid–solid triphase interface in photocatalysis and discuss the working principle of the triphase interface in improving the separation of photogenerated charges and enhancing the reaction efficiency.

In the photocatalytic degradation reaction, the recombination of photogenerated electrons and holes is a major problem that hinders the degradation efficiency. Low-dimensional semiconductors and hybrid photocatalysts are commonly used to improve the separation of electrons and holes.<sup>7–10</sup> However, this strategy can only be used for electrons and holes temporally separated within nanoscale photocatalysts. An effective approach is to remove them from the photocatalyst surface by using suitable and sufficient acceptors. O<sub>2</sub> is an effective natural electron scavenger that can suppress the recombination of photogenerated electrons and holes. However, due to the low concentration and slow diffusion rate of O<sub>2</sub> in aqueous environments, the removal of photogenerated electrons by coupling with O<sub>2</sub> is strongly restricted: this leads to

a low catalytic efficiency and low solar energy efficiency—especially at high pollutant concentrations or high light intensities.

To solve this problem, an air–liquid–solid triphase photocatalytic system is proposed.<sup>11</sup> Fig. 1a shows that TiO<sub>2</sub> nanoparticles are immobilized on a hydrophobic carbon fibre mesh. Once immersed in an aqueous solution, air pockets will form in the empty space of the mesh substrate. Consequently, O<sub>2</sub> can be directly and continuously delivered to the reaction zone, *i.e.*, the aqueous–catalysis interface, from the air phase. This is an efficient route for removing photogenerated electrons from the photocatalyst surface to minimize the recombination of electron–hole pairs even under high light intensity. Fig. 1b shows that the degradation rate and apparent quantum yield of the triphase photocatalytic system are significantly increased *versus* a conventional liquid–solid diphase system—the disparity is more pronounced under high light intensity. It is worth noting that while decomposing the organic molecules in water, the photocatalytic reaction may also break carbon bonds of the superhydrophobic substrate. For practical application, to increase the long-term stability a thick photocatalyst layer or a stable inorganic film that can block the interaction between the reactive oxidizable species and the substrate can be adopted.

H<sub>2</sub>O<sub>2</sub> is an energy carrier and an environmentally friendly oxidant useful in a wide variety of industrial and environmental areas. Photocatalytic H<sub>2</sub>O<sub>2</sub> formation by O<sub>2</sub> reduction has attracted extensive attention because it can proceed under mild conditions (ambient temperature and pressure) and requires only water, O<sub>2</sub>, and excitation light as the material and energy sources. However, due to the low concentration and slow diffusion rate of O<sub>2</sub> in aqueous solution, there is often poor accessibility of O<sub>2</sub> to the catalysts in a normal liquid–solid diphase system. The recombination of photogenerated charges can also impede the electron utilization efficiency. These problems are especially serious when the charge carrier concentrations become higher with increased light intensity; furthermore, the reverse reaction of H<sub>2</sub>O<sub>2</sub> formation, *i.e.*, the degradation of H<sub>2</sub>O<sub>2</sub> by photogenerated electrons may also reduce the product yield.

The air–liquid–solid triphase photocatalytic reaction system can solve these issues and improve the H<sub>2</sub>O<sub>2</sub> production rate.<sup>12</sup> Fig. 1c shows that reactant O<sub>2</sub> can directly and continuously diffuse to the reaction interface from the air phase instead of slowly diffusing through the aqueous solution. This triphase architecture significantly increased the O<sub>2</sub> concentration at the aqueous–catalysis reaction interface and enhanced the removal efficiency of photogenerated electrons by coupling with O<sub>2</sub>. This improves the utilization efficiency of photogenerated charges by suppressing the electron–hole recombination. Besides, the reverse reaction can also be reduced since photogenerated electrons are easily removed by accessible O<sub>2</sub> from the air phase. As a result, a 44-fold enhancement in H<sub>2</sub>O<sub>2</sub> yield can be achieved in the triphase photocatalytic system *versus* the diphase control (Fig. 1d).

Triphase interface photocatalytic reaction systems can also be used to boost plasmon-driven photocatalytic reactions, semiconductor-mediated photodegradation and other photo-



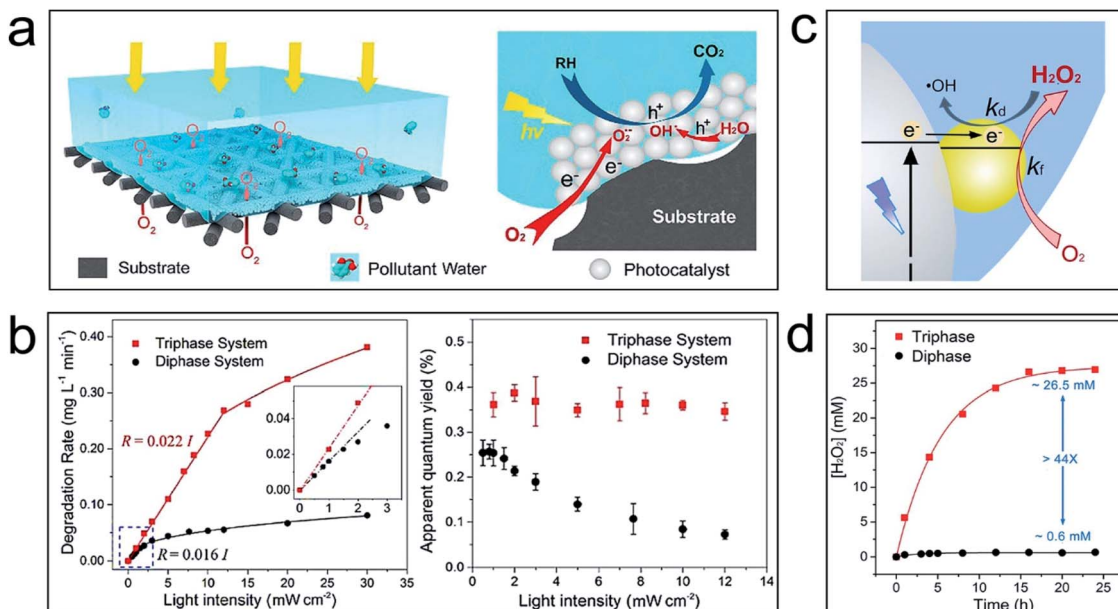


Fig. 1 Application examples of the air–liquid–solid triphase system for photocatalytic reactions. (a) Schematic illustration of the triphase system for degradation of organic pollutants. (b) calibration plots of the degradation rate versus UV light intensity for triphase (red curve) and diphase (black curve) reaction systems (left), and the effect of the UV light intensity on the apparent quantum yield of the triphase and diphase systems (right). Reproduced with permission from ref. 11, Copyright 2017 American Chemical Society. (c) Schematic illustration of formation and degradation reactions of  $\text{H}_2\text{O}_2$  at the triphase interface. (d) The steady-state concentration of  $\text{H}_2\text{O}_2$  produced using the triphase system (red line) and diphase system (black line) under UV light illumination of  $60 \text{ mW cm}^{-2}$ . Reproduced with permission from ref. 12, Copyright 2019 Elsevier.

energy conversion reactions as long as gaseous reactants are involved.<sup>13–16</sup>

## 2.2 Bio-(photo)electrochemical reactions

Oxidase-based bioassays that use natural  $\text{O}_2$  as an electron mediator have great potential in diagnosis of diabetes and other medical problems. Analyte levels can be measured by monitoring either  $\text{O}_2$  consumption or  $\text{H}_2\text{O}_2$  formation (converted from  $\text{O}_2$  in the enzyme-regeneration reaction) that occurs in enzymatic reactions. However, conventional electrode-based biosensors usually operate in environments that contain a liquid–solid diphase interface where  $\text{O}_2$  is supplied from the liquid phase with inherent drawbacks of low solubility, slow diffusion rate, and fluctuating concentration in electrolyte. As a result, the  $\text{O}_2$  required for the enzymatic reaction at the electrolyte–enzyme layer interface is quickly depleted, leading to poor performance with low sensitivity, narrowed detection limits, and poor accuracy.

To address these issues, oxidase-based enzymatic electrodes with an air–liquid–solid triphase interface have been developed.<sup>17</sup> At the top of the sensor electrode (Fig. 2a), an enzyme layer (e.g., glucose oxidase,  $\text{GO}_x$ ) with  $\text{H}_2\text{O}_2$  electrocatalysts (Pt nanoparticles) embedded beneath it maintained good contact with the analyte solution. At the bottom, a superhydrophobic substrate (carbon fibre mesh) traps air when immersed in an aqueous solution. The enzyme catalytic product ( $\text{H}_2\text{O}_2$ ) is electrooxidized on the Pt surface to produce a rapid current response for analyte determination. At the air–liquid–solid triphase interface, the  $\text{O}_2$  required for enzyme regeneration can be

readily provided from the air phase to ensure that a large amount of  $\text{H}_2\text{O}_2$  is formed for accurate analyte determination. In a typical oxidase-based sensing experiment (Fig. 2b), a detection upper limit as high as  $156 \text{ mM}$  towards glucose can be obtained using the triphase biosensor—which is about 30-fold higher than that using the normal diphase one (inset in Fig. 2b). The authors have also studied the long-term stability of the superhydrophobic biosensor by testing its response to a high concentration glucose solution for more than eight months. The biosensor retains its response over the course of 250 days with a variation of less than 5%, indicating good stability of the superhydrophobic bioassay system. Using this triphase design, Mi and co-workers discussed the detailed kinetic parameters of the enzymatic reactions by regulating the constituents of the air phase or dissolved gas in the liquid phase.<sup>18</sup> The results further confirmed the enhancement of the performance of the bioassay *via* the triphase structure.

One lingering issue is selectivity. The photoelectrochemical (PEC) bioassay is an alternative that has attracted growing interest. Compared with electrochemical methods based on  $\text{H}_2\text{O}_2$  oxidation with high oxidation potential, photo-generated holes can oxidize  $\text{H}_2\text{O}_2$  at low overpotential to achieve the same advantages in sensitivity and the linear detection range but with improved selectivity. Nevertheless, similar to electrochemical methods, the  $\text{O}_2$  deficiency problem also hampers normal PEC biosensors with liquid–solid diphase interfaces. Besides, the electron transport in semiconductors may bring new issues for effective charge collection when semiconductor catalysts are used in photoelectrochemical reactions.



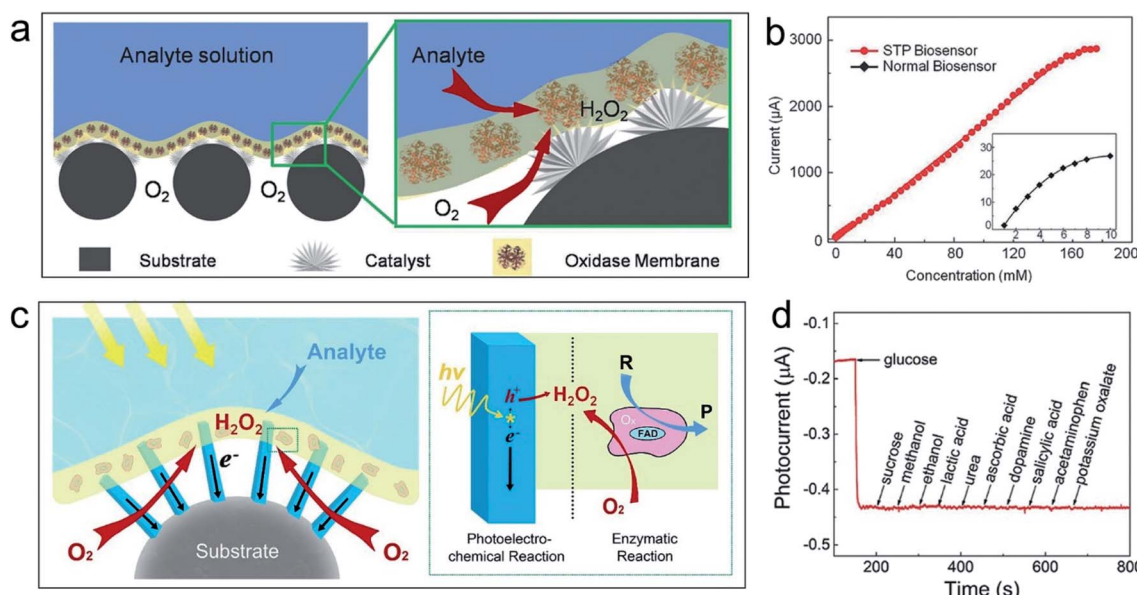


Fig. 2 Application examples of the air–liquid–solid triphase system for bio–(photo)electrochemical reactions. (a) Schematic representation of the triphase biosensor with a thin layer of oxidase/chitosan composite film immobilized on the superhydrophobic substrate that is modified with the  $H_2O_2$  catalyst. The enlarged view shows the air–liquid–solid triphase reaction zone where the oxidase catalytic bioreaction takes place. (b) Calibration plot of the triphase biosensor (red line) and normal diphasic one (black curve in the inset). The linear detection upper limit is 156 mM for the triphase biosensor, which is about 30 times higher than that for the diphasic one (~5 mM). Reproduced with permission from ref. 17, Copyright 2015 Wiley–VCH. (c) Schematic illustration of the air–liquid–solid triphase bio–photoelectrode with a thin oxidase/chitosan composite layer immobilized atop a single-crystal  $TiO_2$  nanowire array film that is grown on a superhydrophobic substrate. The enlarged view shows the triphase reaction zone with rapid and continuous oxygen transport to the reaction interface. R denotes the reactant and P denotes the product. Reproduced with permission from ref. 23, Copyright 2018 Wiley–VCH. (d) Selectivity tests for glucose sensing. The presented curve shows the photocurrent responses for 1 mM glucose and successive addition of 0.1 mM different interferents using the triphase bio–photoelectrochemical assay system based on the reduction method. Reproduced with permission from ref. 26, Copyright 2018 Wiley–VCH.

Single-crystal semiconductor nanowire arrays have excellent electron transport properties *versus* their nanoparticle counterparts.<sup>19–22</sup> A triphase bio-photoelectrochemical assay system based on superhydrophobic substrate supported single-crystal nanowire arrays has been proposed to overcome both the  $O_2$  transport and electron transport limitations.<sup>23,24</sup> As shown in Fig. 2c, a thin oxidase/chitosan composite layer is immobilized atop a single-crystal  $TiO_2$  nanowire array film, which was grown on superhydrophobic carbon cloth. In the presence of  $O_2$ , the  $H_2O_2$  enzymatic product will be generated when the analyte is introduced. Under excitation light irradiation,  $H_2O_2$  can be subsequently oxidized by the photogenerated holes at the semiconductor surface resulting in a photocurrent response in proportion to the analyte level. Consequently, the combination of air–liquid–solid triphase electrode design and arrayed single-crystal nanowires can simultaneously lead to superior gas and charge transport pathways. This increases the upper detection limits and selectivity of the triphase bio-photoelectrochemical sensor at a relatively lower potential.

Based on the discussion above, we know that the (photo)electrochemical oxidation of  $H_2O_2$  is an effective tool for bioassays. However, its inherent drawbacks, *i.e.*, poor selectivity against easily oxidizable interferents, can only be weakened—they cannot be completely eliminated. The (photo)electrochemical reduction method for detecting  $H_2O_2$  is an ideal solution for improving selectivity. Using this method, analytes are determined *via*  $H_2O_2$

reduction at suitable potentials (*e.g.* –0.3 to 0 V *vs.* Ag/AgCl on the Pt catalyst) or with photogenerated electrons. Nevertheless, practical application of the  $H_2O_2$  reduction-based method has been limited because  $O_2$  can also be reduced under the same conditions: this leads to interference currents. The interference current from  $O_2$  reduction will fluctuate because the  $O_2$  level at the traditional electrolyte–catalyst diphasic interface is liquid phase dependent and varies widely. Thus, accurate detection of  $H_2O_2$  by the reduction method is compromised.

The air–liquid–solid triphase joint interface is introduced for bioassays based on the  $H_2O_2$  cathodic reaction.<sup>25,26</sup> Unlike traditional liquid–solid diphasic electrodes, the  $O_2$  level adjacent to the reaction sites is governed by the air phase. Due to the fast and constant  $O_2$  supply for the interfacial reaction centre from the air phase, the  $O_2$  level at the electrolyte–catalyst interface can remain constant and will not be affected by the concentration fluctuation of the dissolved  $O_2$  in the electrolyte. As a result, the interference current caused by the  $O_2$  reduction will stabilize and be treated as a constant signal background; thus, the accuracy of the bioassay based on  $H_2O_2$  reduction can be guaranteed. This leads to a high selectivity of the triphase bioassay. In a bioassay with the air–liquid–solid triphase joint interface, the successive addition of different interferents did not result in any interference signal in the glucose assay (Fig. 2d), which confirmed the practicability of the triphase design for accurate analyte detection.

Other  $O_2$  consumption reactions like the  $O_2$  reduction reaction (ORR) are closely related to energy exploration or environmental governance. These reactions can also use triphase electrodes for performance enhancement. Through rational design, the air–liquid–solid triphase interface can be generated on electrodes assembled using Pt-loaded  $SiO_2$  pillar arrays, nickel foam, N-doped carbon nanotube arrays/nanosheets, or  $Au/NiFeO_x$  modified with a low surface energy material or coated on porous hydrophobic polymer substrates.<sup>27–32</sup> When used in the electrochemical ORR, triphase electrodes with balanced hydrophobicity/hydrophilicity ensured fast gas and ion transport to eventually improve ORR efficiency.

### 3. $N_2$ and $CO_2$ reduction reactions with the triphase interface

The  $N_2$  and  $CO_2$  reduction reactions (NRR and CRR) with photocatalytic or (photo)electrochemical methods can be used for sustainable energy, greenhouse gas elimination, and value-added chemical production.<sup>33,34</sup> In conventional liquid–solid diphase reaction systems, the low dissolution and slow mass transfer of the  $N_2$  and  $CO_2$  in electrolytes seriously restrict the reaction kinetics. Besides, the un-wanted hydrogen evolution reaction (HER)<sup>35–38</sup> will hinder the faradaic efficiency and/or the selectivity of the NRR and CRR. These limitations can be addressed using the air–liquid–solid triphase electrode.

#### 3.1 $N_2$ reduction reactions

The use of the (photo)electrochemical NRR to produce  $NH_3$  is a particularly promising technique because the  $NH_3$  product is heavily used in chemical and pharmaceutical production, and is also a potential carbon-free energy carrier. However, in aqueous solutions, the (photo)electrochemical NRR is inhibited by the intense competition from the HER of water that results from the preferential adsorption of protons over nitrogen across all traditional NRR catalysts. Furthermore, once water exists in the reaction system (even the trace atmospheric water vapor), the HER will occur and generate dominant (photo)electrochemical current interference. Therefore, the intrinsic NRR (photo)electrochemical features can hardly be detected, let alone the further thermodynamic or kinetic studies.

To achieve the (photo)electrochemical NRR with high selectivity and high efficiency under ambient conditions, an air–liquid–solid triphase photoelectrode structure is designed.<sup>39</sup> As shown in Fig. 3a, a hydrophobic layer of the porous polytetrafluoroethylene (PTFE) framework was covered on the  $Ti-Si$  substrate with  $Au$  nanoparticles uniformly distributed on the framework. When the photoelectrode was immersed in electrolyte, an air phase will form by trapping gaseous  $N_2$  in the porous PTFE framework. Fig. 3b shows that the yield rate of  $NH_3$  (NRR product) and faradaic efficiency using the triphase electrode ( $Au$ –PTFE/TS) are higher than those using the diphase one ( $Au$ /TS) in a wide potential range. The excellent performance of the triphase reaction system can be ascribed to the direct transport of  $N_2$  molecules to the surface of the catalyst ( $Au$  nanoparticles) from the air phase. The hydrophobicity of the

electrode ensured a low water contact area, which consequently restricts the contact between the proton and the catalysts. Eventually, the HER is suppressed, and the efficiency of the NRR is improved. Similar results for improving the NRR performance with electrochemical methods have been reported by constructing triphase interfaces with hydrophobic layers of the zeolitic imidazolate framework (ZIF) over the NRR electrocatalyst surfaces,<sup>40,41</sup> indicating that the strategy of constructing electrodes with a triphase interface is feasible for the NRR under mild conditions.

#### 3.2 $CO_2$ reduction reactions

The photocatalytic or electrochemical CRR can eliminate greenhouse gases and harvest renewable resources. In the ideal case, both the hydrogen ion and  $CO_2$  source for the CRR can be supplied from the aqueous solution. However, in most cases, the dominant reaction in aqueous solution is the competing HER, *i.e.*, direct water reduction by capturing photo-generated electrons or at cathodic polarized potentials. This leads to low selectivity and low activity of the CRR. Therefore, it is highly desirable to create an environment that simultaneously suppresses the HER and enhances the CRR.

Among the different strategies for tackling this problem, a simple solution by constructing an air–liquid–solid triphase reaction interface has been proposed.<sup>42</sup> Fig. 3c shows that an efficient triphase contact of  $CO_2$  (air phase),  $H_2O$  (liquid phase), and the catalyst (solid phase) is formed by modifying polymeric carbon nitride nanosheets with a hydrophobic polymer (with/without  $Pt$  nanoparticle loading). At the triphase joint interface, concentrated  $CO_2$  molecules in the air phase can directly transport to the surface of photocatalysts, which removes the mass-transfer limitations of  $CO_2$ . The hydrophobic surface lowers the hydrogen ion contacts and suppresses the HER. In the photocatalytic  $CO_2$  reduction experiments (Fig. 3d), the hydrophobic catalysts ( $o$ -PCN) have high selectivity towards carbon-containing compounds, and a negligible amount of hydrogen is detected. This phenomenon becomes more pronounced even when  $Pt$  nanoparticles—one of the most efficient electron-collection agents and HER-promotion cocatalysts—are loaded for the photocatalytic reaction. These results proved the superior performance of the air–liquid–solid triphase interface and can improve the efficiency and selectivity of the photocatalytic CRR.

Electrochemical  $CO_2$  reduction is also a simple approach with great potential for the CRR. Similar to photocatalytic activities, the competitive HER predominates when cathodic polarization occurs in an aqueous environment. In addition, the reduction of extremely stable  $CO_2$  molecules is kinetically sluggish, and relatively high overpotentials are required. These features lead to low selectivity and low faradaic efficiency for  $CO_2$  reduction.

Wakerley and co-workers recently prepared an air–liquid–solid triphase electrode by modifying hierarchically structured  $Cu$  dendrites with 1-octadecanethiol—a low surface energy compound.<sup>43</sup> Fig. 3e shows that once immersed in electrolyte, the assembled hydrophobic electrode with the triphase joint



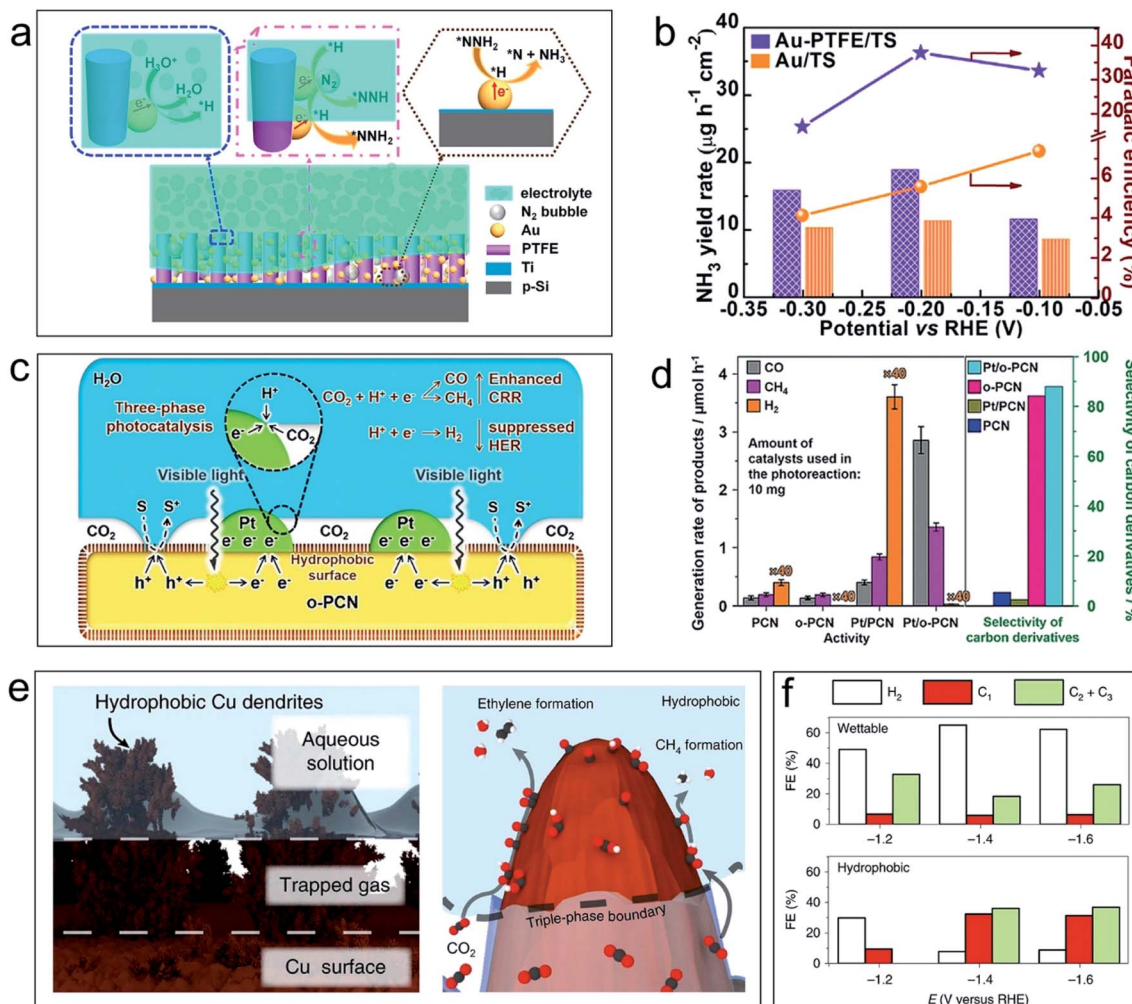


Fig. 3 Application examples of the air–liquid–solid triphase system for the NRR and CRR. (a) Schematic illustration and the proposed reaction route of the triphase system for the electrochemical NRR on the Si-based photocathode. (b) Yield rate of  $\text{NH}_3$  (column diagrams) and faradaic efficiency (point plots) on Au/TS (orange) and Au-PTFE/TS (purple) at each given potential for 4 hours (TS denotes a thin Ti layer on the Si surface). Reproduced with permission from ref. 39, Copyright 2018 Elsevier. (c) Scheme of the triphase photocatalyst (hydrophobic polymeric carbon nitride nanosheets loaded with Pt nanoparticles) and the mechanism of the triphase photocatalytic CRR. S represents the hole sacrificial agent, and  $\text{S}^+$  represents the sacrificial agent which is oxidized by holes. (d) The activity of the photocatalytic CRR and selectivity towards carbon derivatives with the catalysts polymeric carbon nitride (PCN) and hydrophobic polymeric carbon nitride (o-PCN) with/without Pt partial loading. The note  $\times 40$  means the value of this column shown here is reduced by 40 times. Reproduced with permission from ref. 42, Copyright 2019 Wiley-VCH. (e) The illustration of the air–liquid–solid triphase interface when a hydrophobic Cu dendrite placed in water and gas trapped between dendrites (left), and the enhanced  $\text{CO}_2$  mass transport from the triple-phase boundary between the electrolyte, electrode and gaseous  $\text{CO}_2$  and the resultant formation of key products on the surface (right). (f) Controlled potential electrolysis product faradaic efficiencies from the wettable (diphasic interface) and hydrophobic (triphasic interface) dendrites at various potentials. Reproduced with permission from ref. 43, Copyright 2019 Springer Nature.

interface can trap gaseous  $\text{CO}_2$  in the empty space of the Cu dendrites. During the electrochemical reduction process, gaseous  $\text{CO}_2$  in the air phase can be directly and continuously delivered to the reaction interface. This removes the transportation barriers of  $\text{CO}_2$  in aqueous phases and largely improves the  $\text{CO}_2$  concentration near the reaction centre. Meanwhile, the hydrophobic surface of the electrode minimized the water contact area and thus suppressed the HER. As a result, the electrochemical CRR with lowered HER efficiency and increased faradaic efficiency towards value-added carbon-containing chemicals is achieved (Fig. 3f). Using the same design

principle, the triphase interface is constructed by modifying the catalyst ( $\text{MoS}_2$  nanosheets) with hydrophobic fluorosilane molecules or depositing gold nanoparticles on a hydrophobic nanoporous polyethylene membrane.<sup>44,45</sup> This can also improve the CRR efficiency and enhance the electrochemical stability.

#### 4. Conclusions and outlook

We briefly introduced the most recent progress in heterogeneous reactions involving gas consumption at air–liquid–solid triphase interfaces. By integrating hydrophobic materials with



traditional hydrophilic catalysts, delicately designed triphase catalytic systems can be formed once the reactions occur in aqueous solution. At the triphase interface, gaseous reactants can be rapidly and constantly supplied to the reaction centre from the air phase. This removes barriers of low solubility and slow transport of gaseous reactants in traditional liquid–solid diphase systems. Furthermore, the hydrophobic surface of the catalysts can decrease the contact area for the hydrogen ion, which suppresses the competing hydrogen evolution reaction during  $\text{CO}_2$  or  $\text{N}_2$  reduction reactions.

In this minireview, enhanced photocatalytic, bioelectronic and (photo)electrochemical reactions have been demonstrated using the rationally designed and constructed triphase system. However, only a few gas consumption reactions are covered in these reports of progress. Thus, it is intriguing to further explore the fundamental roles of the air–liquid–solid triphase interface in other interesting and valuable reactions. For example, the hydrogenation reaction is one of the most important reactions in the fine chemical and pharmaceutical industry. Applying the triphase reaction system to the liquid hydrogenation reaction could be an efficient way to increase  $\text{H}_2$  concentration on the catalyst surface, thus enhancing the hydrogenation reaction rate. Moreover, by rational design the triphase interface can also be used in gas evolution reactions like solar/electro-driven water splitting for  $\text{H}_2$  or  $\text{O}_2$  evolution. Given the wide variety of gaseous reactants involved in these reactions, the air–liquid–solid triphase reaction system could be used as a promising platform for environmental treatment, clean energy, value-added chemical production, and biological and clinical diagnosis.

## Conflicts of interest

There are no conflicts to declare.

## Acknowledgements

We acknowledge financial support from the National Natural Science Foundation of China (21988102 and 51772198) and the Jiangsu Province Science Foundation for Distinguished Young Scholars (BK20150032).

## Notes and references

- 1 P. Sudarsanam, E. Peeters, E. V. Makshina, V. I. Parvulescu and B. F. Sels, *Chem. Soc. Rev.*, 2019, **48**, 2366–2421.
- 2 Z. Wang, C. Li and K. Domen, *Chem. Soc. Rev.*, 2019, **48**, 2109–2125.
- 3 J. Wang, *Chem. Rev.*, 2008, **108**, 814–825.
- 4 B. Garlyyev, J. Fichtner, O. Piqué, O. Schneider, A. S. Bandarenka and F. Calle-Vallejo, *Chem. Sci.*, 2019, **10**, 8060–8075.
- 5 W. Barthlott and C. Neinhuis, *Planta*, 1997, **202**, 1–8.
- 6 Y. Wu, J. Feng, H. Gao, X. Feng and L. Jiang, *Adv. Mater.*, 2019, **31**, e1800718.
- 7 L. Wei, C. Yu, Q. Zhang, H. Liu and Y. Wang, *J. Mater. Chem. A*, 2018, **6**, 22411–22436.

- 8 C. Liu, D. S. Kong, P. C. Hsu, H. T. Yuan, H. W. Lee, Y. Y. Liu, H. T. Wang, S. Wang, K. Yan, D. C. Lin, P. A. Maraccini, K. M. Parker, A. B. Boehm and Y. Cui, *Nat. Nanotechnol.*, 2016, **11**, 1098–1104.
- 9 S. Selim, L. Francàs, M. García-Tecedor, S. Corby, C. Blackman, S. Gimenez, J. R. Durrant and A. Kafizas, *Chem. Sci.*, 2019, **10**, 2643–2652.
- 10 B. Song, Q. Wang, L. Wang, J. Lin, X. Wei, V. Murugadoss, S. Wu, Z. Guo, T. Ding and S. Wei, *J. Colloid Interface Sci.*, 2020, **559**, 124–133.
- 11 X. Sheng, Z. Liu, R. Zeng, L. Chen, X. Feng and L. Jiang, *J. Am. Chem. Soc.*, 2017, **139**, 12402–12405.
- 12 Z. Liu, X. Sheng, D. Wang and X. Feng, *iScience*, 2019, **17**, 67–73.
- 13 H. Zhou, X. Sheng, J. Xiao, Z. Ding, D. Wang, X. Zhang, J. Liu, R. Wu, X. Feng and L. Jiang, *J. Am. Chem. Soc.*, 2020, **142**, 2738–2743.
- 14 Y. Gao, N. Yang, S. Lu, T. You and P. Yin, *J. Mater. Chem. C*, 2019, **7**, 9926–9932.
- 15 D. Aebisher, D. Bartusik, Y. Liu, Y. Zhao, M. Barahman, Q. Xu, A. M. Lyons and A. Greer, *J. Am. Chem. Soc.*, 2013, **135**, 18990–18998.
- 16 J. Liu, L. Ye, S. Wooh, M. Kappl, W. Steffen and H.-J. Butt, *ACS Appl. Mater. Interfaces*, 2019, **11**, 27422–27425.
- 17 Y. Lei, R. Sun, X. Zhang, X. Feng and L. Jiang, *Adv. Mater.*, 2016, **28**, 1477–1481.
- 18 L. Mi, J. Yu, F. He, L. Jiang, Y. Wu, L. Yang, X. Han, Y. Li, A. Liu, W. Wei, Y. Zhang, Y. Tian, S. Liu and L. Jiang, *J. Am. Chem. Soc.*, 2017, **139**, 10441–10446.
- 19 J. Liu, X. Sheng, F. Guan, K. Li, D. Wang, L. Chen and X. Feng, *Chem. Sci.*, 2018, **9**, 7400–7404.
- 20 X. Sheng, L. Chen, T. Xu, K. Zhu and X. Feng, *Chem. Sci.*, 2016, **7**, 1910–1913.
- 21 X. Feng, K. Zhu, A. J. Frank, C. A. Grimes and T. E. Mallouk, *Angew. Chem., Int. Ed.*, 2012, **51**, 2727–2730.
- 22 X. Sheng, D. He, J. Yang, K. Zhu and X. Feng, *Nano Lett.*, 2014, **14**, 1848–1852.
- 23 L. Chen, X. Sheng, D. Wang, J. Liu, R. Sun, L. Jiang and X. Feng, *Adv. Funct. Mater.*, 2018, **28**, 1801483.
- 24 D. Wang, L. Chen, Z. Ding and X. Feng, *Sol. RRL*, 2019, DOI: 10.1002/solr.201900185.
- 25 Z. Song, C. Xu, X. Sheng, X. Feng and L. Jiang, *Adv. Mater.*, 2018, **30**, 1701473.
- 26 D. Wang, L. Chen, J. Liu, F. Guan, R. Sun, L. Jiang and X. Feng, *Adv. Funct. Mater.*, 2018, **28**, 1804410.
- 27 P. Wang, T. Hayashi, Q. a. Meng, Q. Wang, H. Liu, K. Hashimoto and L. Jiang, *Small*, 2017, **13**, 1601250.
- 28 K. Xu, A. Loh, B. Wang and X. Li, *J. Electrochem. Soc.*, 2018, **165**, A809–A818.
- 29 Y. Li, H. Zhang, N. Han, Y. Kuang, J. Liu, W. Liu, H. Duan and X. Sun, *Nano Res.*, 2019, **12**, 177–182.
- 30 J. Li, Y. Zhu, W. Chen, Z. Lu, J. Xu, A. Pei, Y. Peng, X. Zheng, Z. Zhang, S. Chu and Y. Cui, *Joule*, 2019, **3**, 557–569.
- 31 Y. Zhai, J. Wang, Q. Gao, Y. Fan, C. Hou, Y. Hou, H. Liu, Q. Shao, S. Wu, L. Zhao, T. Ding, F. Dang and Z. Guo, *J. Catal.*, 2019, **377**, 534–542.



32 W. Zhao, X. Li, R. Yin, L. Qian, X. Huang, H. Liu, J. Zhang, J. Wang, T. Ding and Z. Guo, *Nanoscale*, 2019, **11**, 50–59.

33 W. Guo, K. Zhang, Z. Liang, R. Zou and Q. Xu, *Chem. Soc. Rev.*, 2019, **48**, 5658–5716.

34 S. Fukuzumi, Y.-M. Lee, H. S. Ahn and W. Nam, *Chem. Sci.*, 2018, **9**, 6017–6034.

35 G. Zheng, J. Wang, G. Zu, H. Che, C. Lai, H. Li, V. Murugadoss, C. Yan, J. Fan and Z. Guo, *J. Mater. Chem. A*, 2019, **7**, 26077–26088.

36 C. Wang, F. Lan, Z. He, X. Xie, Y. Zhao, H. Hou, L. Guo, V. Murugadoss, H. Liu, Q. Shao, Q. Gao, T. Ding, R. Wei and Z. Guo, *ChemSusChem*, 2019, **12**, 1576–1590.

37 J. Desai, P. Baviskar, K. Hui and H. Pathan, *ES Energy Environ.*, 2018, **2**, 21–30.

38 S. Guo, J. Shang, T. Zhao, D. Hou, Z. Jin and G. Sun, *ES Mater. Manuf.*, 2018, **2**, 24–27.

39 J. Zheng, Y. Lyu, M. Qiao, R. Wang, Y. Zhou, H. Li, C. Chen, Y. Li, H. Zhou, S. P. Jiang and S. Wang, *Chem*, 2019, **5**, 617–633.

40 H. K. Lee, C. S. L. Koh, Y. H. Lee, C. Liu, I. Y. Phang, X. Han, C.-K. Tsung and X. Y. Ling, *Sci. Adv.*, 2018, **4**, eaar3208.

41 J. Liu, R. Li, X. Zu, X. Zhang, Y. Wang, Y. Wang and C. Fan, *Chem. Eng. J.*, 2019, **371**, 796–803.

42 A. Li, Q. Cao, G. Zhou, B. Schmidt, W. Zhu, X. Yuan, H. Huo, J. Gong and M. Antonietti, *Angew. Chem., Int. Ed.*, 2019, **58**, 14549–14555.

43 D. Wakerley, S. Lamaison, F. Ozanam, N. Menguy, D. Mercier, P. Marcus, M. Fontecave and V. Mougel, *Nat. Mater.*, 2019, **18**, 1222–1227.

44 K. Lv, C. Teng, M. Shi, Y. Yuan, Y. Zhu, J. Wang, Z. Kong, X. Lu and Y. Zhu, *Adv. Funct. Mater.*, 2018, **28**, 1802339.

45 J. Li, G. Chen, Y. Zhu, Z. Liang, A. Pei, C.-L. Wu, H. Wang, H. R. Lee, K. Liu, S. Chu and Y. Cui, *Nat. Catal.*, 2018, **1**, 592–600.

